Observation of a Non-Constant Mean Curvature Interface in an ABC Triblock Copolymer

Samuel P. Gido,† Dwight W. Schwark,‡ and Edwin L. Thomas*

Departments of Chemical Engineering and Materials Science & Engineering, Massachusetts Institute of Technology, Cambridge, Massachusetts 02139

Maria do Carmo Gonçalves

Instituto de Química, Universidade Estadual de Campinas, Campinas, São Paulo 13081, Brazil

Received September 14, 1992
Revised Manuscript Received February 3, 1993

Block copolymers are material systems of great technological importance in which a chain of N_A units of monomer A is covalently linked to a chain of N_B units of monomer B. The thermodynamic driving force for phase separation between the two unlike blocks leads to periodic microphase-separated, composite structures which impart novel mechanical and transport properties.[1-5] The interfacial region between the different blocks has been shown experimentally to be about 20 Å thick[6-10] and can thus be approximated as a two-dimensional surface when compared to the size of the microdomains which are several hundred or more angstroms thick. Many previous direct observations via transmission electron microscopy (TEM) of the equilibrium microphase-separated structures that form have shown that the intermaterial dividing surface (IMDS) between the two microphases is a surface of approximately constant mean curvature (CMC). Mean curvature is defined as the arithmetic average of the two principal curvatures (which are the reciprocals of the two principal radii of curvature) at any point on the IMDS, and CMC surfaces represent local interfacial area minima under fixed volume constraints. In diblock copolymers the occurrence of the following equilibrium, CMC morphologies has been well documented: spheres, cylinders, ordered bicontinuous double diamond (OBDD), and lamella. Additionally grain boundary structures have been observed to have CMC or minimal surface geometries.[11,12] Finally, other unusual CMC structures such as the lamellar catenoid structure[11] and the mesh phase[13] have been recently observed in block copolymers. We now report the observation of an interfacial surface in a well-ordered, microphase-separated, amorphous ABC triblock copolymer morphology that is not area minimizing and distinctly non-CMC.

The incompatibility between the A and B blocks is quantified by an interfacial energy or tension γ which acts at the IMDS and is simply related to the Flory-Huggins χ parameter.[14,15] If this interfacial term were the only variable to be minimized in the free energy of the block copolymer, then the physical situation would be exactly represented by the mathematical problem of minimizing surface area with respect to fixed volume constraints. CMC surfaces are *local* solutions to this mathematical problem.[11,16] However, in the actual block copolymer system, additional terms are present in the free energy functional. The most significant of these is the conformational energy of the polymer chains as they are stretched or compressed, normal to the IMDS, from their preferred random-coil shape. Charvolin and Sadoc[17,18] have described the inability of a molecular assembly to simultaneously satisfy a preferred, uniform interfacial curvature and a constant, chain dimension dependent, interdomain spacing as "frustration". This competition between interface shape and the chain-packing conformation is fundamentally important to the appearance of a succession of periodic microdomain morphologies with variation of copolymer composition.[19]

There is also a term in the free energy of the system resulting from the loss of translational entropy which occurs when the diblocks are required to locate their junction points on the IMDS. This term, which scales as the logarithm of the ratio of the volume available to the junctions in the region of the IMDS to the volume of the entire system,[20,21] is negligible with respect to interfacial and chain conformational energies. The presence of the chain conformational term indicates that, mathematically, the equilibrium structures observed in block copolymer morphologies may not have *exactly* CMC interfacial surfaces. Many micrographs of poorly ordered diblock systems show domains with apparent variable curvature of their IMDS. Indeed, some micrographs even suggest the presence of sharp corners. However, we believe such images are a result of the far-from-equilibrium conditions suggested by the poor overall domain organization and/or from superposition of a three-dimensional interface structure in the two-dimensional image projections.

The IMDS of the cylindrical diblock morphology appears circular when viewed in projection down the cylindrical axis. However, as indicated in Figure 1, the requirement that the chain packing in the Wigner-Seitz (W-S) cell around the cylinder preserve constant segmental density leads to an azimuthal dependence of the outer block chain conformation. An examination of published lattice parameters and cylindrical radii for cylinder-forming block copolymers in the literature[2,22-24] shows that the cylindrical core blocks are stretched by about 10-40% of their unperturbed end-to-end distance. The amount of stretching in each case depends upon composition, molecular weight, and also the extent to which the sample preparation techniques allowed the samples to approach the equilibrium structure.

The corona block chain conformations are a more difficult subject. The average corona thickness may be calculated by determining the thickness of the cylindrical annulus which has a volume equal to that of the actual W-S cell minus the cylindrical core. This average corona thickness is smaller than the unperturbed root-mean-square end-to-end distance of the corona block. On this basis one might conclude that the corona block chain conformations are compressed. However, by using this measure of corona thickness we are making the implicit assumption that there is little or no overlapping of the chains in the coronas of adjacent cylinders. The compressed chain conformations that result from the assumption of nonoverlapping coronas are shown on the left-hand side of Figure 1. Semenov[19] has suggested that it may be energetically favorable for the coronas of closely packed spherical and cylindrical micelles to strongly overlap. This situation is illustrated on the right-hand side of Figure 1. In the case of strong corona overlap the outer block chains are stretched. Results of rheological studies[25] indicate that there is surely some overlap of the micellar coronas, but a quantitative measure of the extent of overlap, and

* To whom correspondence should be addressed.
† Present address: Department of Polymer Science and Engineering, University of Massachusetts, Amherst, MA 01003.
‡ Present address: Eastman Kodak Co., Rochester, NY 14652-3712.

0024-9297/93/2226-2636$04.00/0

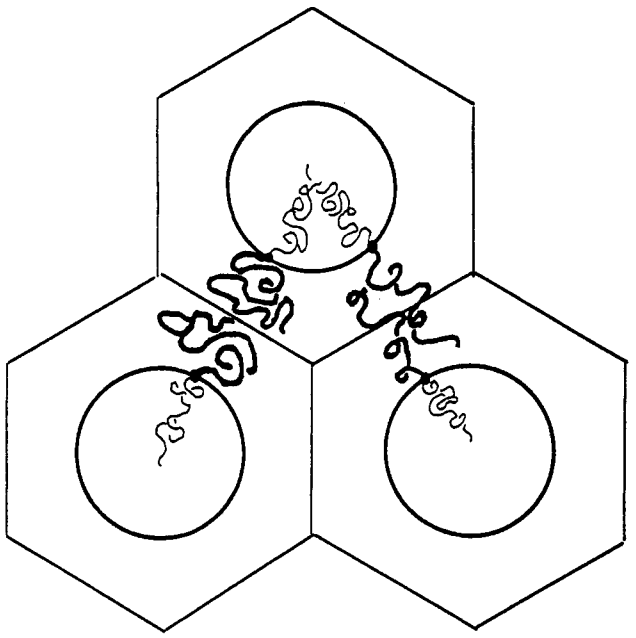

Figure 1. Axial view of corona block conformations in the cylindrical morphology. The thickness of the corona region is smaller than the root-mean-square end-to-end distance of the corona block. This may lead, as shown on the left, to compression of the corona block. If, however, as shown on the right, there is significant overlap of the coronas of neighboring cylinders, then the corona blocks may be stretched.

its effect on chain conformation, is to date unavailable. The important point is that, regardless of whether the corona blocks are compressed or stretched, this conformational perturbation is a function of the azimuthal angle around the cylinder axis.

Additionally, the comparison between the unperturbed end-to-end distance and the corona thickness makes the implicit assumption that the corona thickness is a good approximation to the end-to-end distance of the outer blocks in the microphase-separated state. Self-consistent-field calculations on grafted polymer layers[26] indicate that not all chains reach the full height of a grafted layer such as the corona of our cylinders. However, in a neat diblock system such as that discussed here, the great majority of the chains have their free end located near the full brush height. Further, in a neat brush grafted to the convex side of a cylinder, as our corona chains are, the tendency of the free chain ends to collect at the outer edge of the brush is further enhanced by the greater available volume at greater distances from the interface.[27]

Referring again to Figure 1, notice that, regardless of whether one uses an overlapping or a nonoverlapping model, the chains near the extreme points of the Wigner–Seitz cell boundary must experience different chain conformations from those chains near the midpoints of the flat sides of the cell. For instance, in the nonoverlapping scenario the chains near the corners experience less chain conformational compression while chains in regions near the middle of the sides of the cell must experience more compression. In the overlapping scenario the chains near the corners are more stretched than those near the sides. We might expect some of this uneveness in chain conformation to be transferred to the IMDS. In fact, such nonuniform chain conformational requirements suggest that the IMDS must deviate from CMC. However, for diblocks of cylindrical domain structure the deviations from perfect CMC interfacial structure are too small to be detected with TEM. Similarly, any deviations of the physical IMDS's from the model CMC structures are too small to detect in the spherical[10] and OBDD[28,29] morphologies.

We were able to obtain a morphology in which the IMDS is distinctly non-CMC utilizing an ABC triblock copolymer. As shown in the TEM micrograph of Figure 2a, the IMDS has corners. The triblock consisted of 33 vol % poly(2-vinylpyridine) (P2VP), linked to 33 vol % polyisoprene (PI), linked to 33 vol % polystyrene (PS). The molecular weights of the P2VP, PI, and PS blocks were 15 100, 13 000, and 14 900, respectively. The sample was slowly cast into a ~1-mm-thick film from THF solution, annealed for a week at 120 °C, and prepared for TEM observation by cryoultramicrotomy and selective staining with OsO_4 and/or CH_3I.[30] In Figure 2a, the CH_3I-stained P2VP blocks are in the gray central cylindrical cores of the hexagonally packed structural units, which are oriented normal to the plane of the micrograph. Surrounding the cylindrical core of P2VP there is a shell of PI which appears dark in the micrograph due to staining with OsO_4. The outer interface of this PI shell, which separates it from the PS matrix material, has the shape of a hexagonal prism with flat sides and fairly sharp edges. This appears as a regular hexagon in the axial projection. Figure 2b shows a transverse view of the ABC microdomain structure. The three different contrast levels evident arise from the superposition of the coaxial cylindrical structure. The lightest layer corresponds to a projection through the unstained continuous PS matrix, the two darkest layers to the outer regions of the OsO_4-stained PI annulus, and the intermediate gray region to the superposition of the central PI region and the CH_3I-stained P2VP core. The hexagonal packing of these coaxial cylindrical units, coupled with chain conformational energies, leads to this pseudohexagonal interface structure which is not area minimizing and is distinctly non-CMC. A coaxial cylindrical morphology was first suggested for an ABC triblock by Riess et al.[31]

In order to explain this non-CMC interface, a very simple model for the structure of the system is utilized. Although there are two types of interfaces in the material, between P2VP and PI and between PI and PS, we will only include the outer one between PI and PS in the model since this is the one whose shape we wish to investigate. We thus lump the two inner blocks (P2VP and PI) together as a single entropy spring while considering the outer PS block separately. Other free energy contributions, the entropic terms related to localization of the junctions between the blocks on the IMDS and the packing of the units into the hexagonal array, are much smaller[19,22,32] and are neglected. We would need a more complete free energy expression if we wished, for instance, to compare the thermodynamic stability of the observed structure with other possible morphologies for this triblock. For instance, Mogi et al.[33,34] found an ABCCBA three-component lamellar morphology for a PI/PS/P2VP triblock of very similar composition and molecular weight also cast from THF solution. The only difference between their system and ours was in the order of connectivity of the three blocks. The difference in block sequence results in A–C rather than B–C type interactions in our triblock. The model used in this paper is not able to address the energetic difference between their triblock structure and ours. However, our simplified model is sufficient for the present purpose of understanding the shape of the PI–PS IMDS.

Although more accurate calculations of chain conformational energy are available,[19,26] the following simple scaling relationships for the free energy per chain, F, are accurate to within a constant factor of order unity[35] and

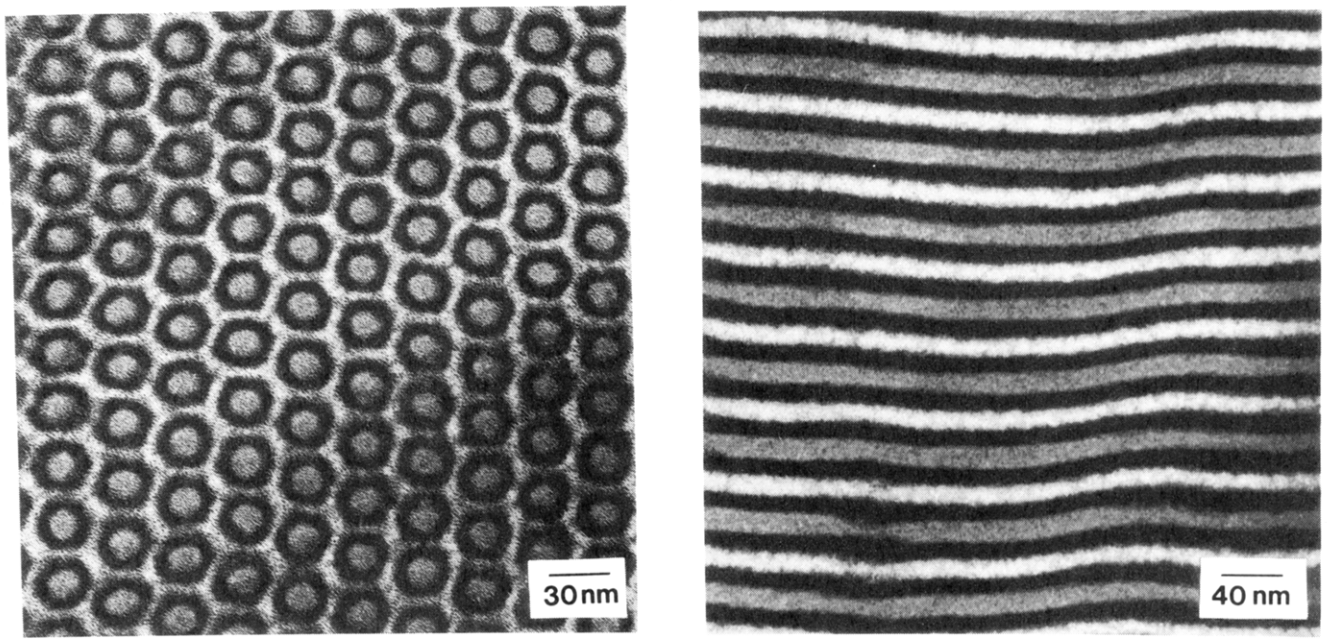

Figure 2. (a) Axial TEM projection of hexagonally packed structural units. The darkest regions correspond to the OsO_4-stained PI domains, while the gray regions are CH_3I-stained P2VP domains. The non-CMC interface between this PI microdomain and the PS matrix phase has a hexagonal shape with corners. (b) Transverse TEM projection. The light, gray, and dark regions correspond to projections through the PS matrix, the P2VP core, and the PI annulus, respectively.

are thus sufficient for our purposes.

$$F = F_i + F_{c1} + F_{c2} \tag{1}$$

F_i is the interfacial energy per chain at the PS–PI interface given by $F_i = \gamma A$. Here γ is the interfacial energy per unit area of IMDS and A is the area per chain junction on this interface. γ for the PS–PI interface is about $0.012\ kT/Å^2$ at 120 °C, the annealing temperature at which the microstructure was formed.[36] F_{c1} and F_{c2} are conformational energies per chain for the combined P2VP–PI blocks and for the PS block, respectively. They are approximated by the following expression:[32,37-39]

$$F_{cj} = \frac{3}{2}k_B T\left\{\left(\frac{R_j}{R_{j0}}\right)^2 + \left(\frac{R_{j0}}{R_j}\right)^2 - 2\right\} \tag{2}$$

where j is an index referring to (1) the combined inner two blocks or (2) the outer PS block. R_j is the end-to-end distance of block j in the microphase-separated morphology. In the Alexander–de Gennes formalism this end-to-end distance is taken as the thickness of the layer in the structure corresponding to block j. Thus for the inner combined block this distance is taken to be from the center of the P2VP cylinder to the IMDS separating PI and PS (assumed to be constant, since the percent variation in this length is quite small). For the outer block this end-to-end distance is approximated, in the noninterpenetrating case, as the azimuthally dependent distance from the PI–PS IMDS to the boundary of the Wigner–Seitz cell. R_{j0} is the ideal Gaussian chain end-to-end distance of the j block, which is the reference state for chain conformational energy and which is given by $a_j N_j^{1/2}$, where N_j is the degree of polymerization of block j and a_j is the statistical segment length of the polymer in block j. For the inner, combined block a_j was taken as the arithmetic average of the P2VP and PI statistical segment lengths while N_j was taken as the sum of the P2VP and PI degrees of polymerization. Equation 2 has the form of the energy penalty for the deformation of an elastic entropy spring, where the first term in parentheses accounts for tension and the second term accounts for compression.

The effect of the conformational and interfacial energies on the PI–PS IMDS shape was simulated using K. Brakke's Surface Evolver software.[40] This software allows a simulated interfacial surface to evolve from an arbitrary initial state to its equilibrium geometry. Surface evolution is driven by user-specified energetic potentials (eqs 1 and 2) and is subject to specified physical constraints such as fixed volume fractions. The computational methods employed by the Surface Evolver are described in ref 40. In our implimentation we worked with the triangular section of the triblock morphology outlined in Figure 3a. This triangle is a $^1/_{12}$ wedge of the Wigner–Seitz cell, and it is the smallest unit which represents the full geometry of the material. The triangle is assumed to have unit depth into the plane of the figure so that all lengths measured on the triangle have units of area. Within this triangle the PI–PS interface was initially approximated as a straight line of arbitrary placement and direction. Then through successive iterations of the calculation, the surface is refined, i.e., divided into a greater number of finite elements which, in our simple two-dimensional problem, were line segments. The points joining these line segments are known as vertices. In each round of the iteration, the gradient of the free energy potential is calculated at each vertex. Each vertex is then moved in the direction which was locally determined to be the direction of greatest energy reduction for that particular vertex. These motions are subject to constraints such as the maintenance of surface continuity and user-specified volume fractions.

The interfacial and chain conformational energies then drive changes in interfacial shape and position so as to minimize free energy while satisfying the fixed volume constraints imposed by triblock volume fractions. Equation 2 gives a local azimuthally dependent conformational energy per chain. This chain energy is scaled by the ratio of the surface area of the elements used in the Surface

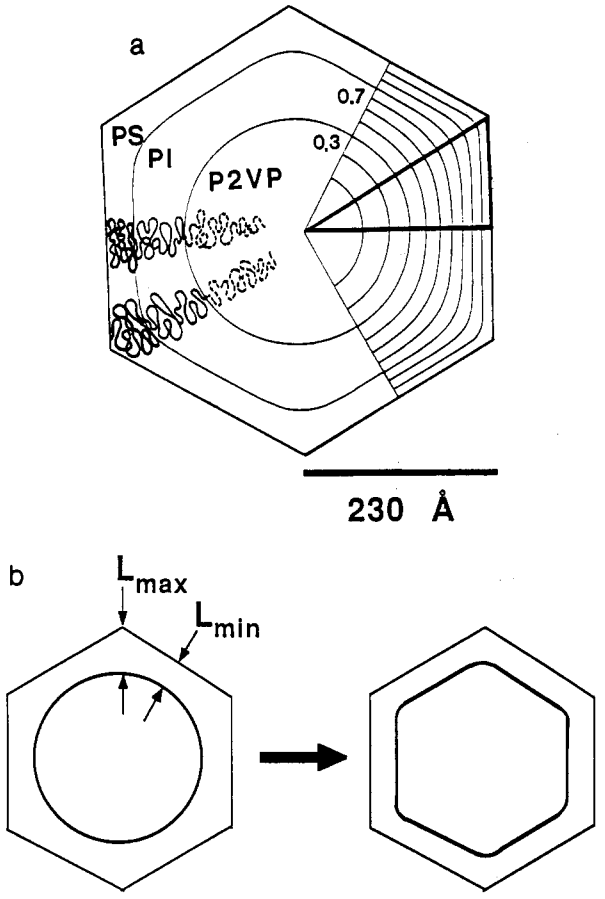

Figure 3. (a) Schematic diagram of the triblock morphology. Surface Evolver calculations of the IMDS shape were carried out for the volume in the bold triangle and extended to the full structural unit by symmetry. A series of interface shapes are shown, with the volume fraction of the inner material increasing in increments of 0.1. The two profiles that are continued completely around the structural unit correspond to volume fractions of ~0.3 and ~0.7 for the total material contained within them. These two profiles correspond to the P2VP–PI and PI–PS interfaces, respectively. (b) Criteria for the formation of non-CMC interfaces in block copolymers. On the left is shown the W–S cell of a periodic block copolymer structure, a hexagon in this case. The circle illustrates the logical choice for a CMC IMDS. If, however, $(L_{max} - L_{min})/L_{av}$ is about 0.7 or greater, then a non-CMC interface may be formed as indicated on the right.

Evolver calculation to the area per chain. This appropriately distributes the chain stretching energy so that integration of this energy over a number of surface elements, which add up to give the IMDS area of a single chain, yields the conformational energy of a single chain. The physical dimensions of the simulation triangle in angstroms and the area per chain on the IMDS were required for these calculations. The dimensions of the morphology (indicated in Figure 3a) were found by small-angle X-ray scattering (SAXS), and the areas per chain were calculated from this SAXS data, the triblock composition, and polymer densities. These areas were 370 Å^2 per chain for the P2VP–PI interface and 520 Å^2 per chain for the PI–PS interface, although we only used the PI–PS interface value in our calculations.

A family of curves representing the PI–PS interface are shown on the triangle in Figure 3a. These curves, from the domain center outward, represent the PI–PS interface for decreasing PS volume fraction. The complimentary, inner, volume is assumed to be equally partitioned between the P2VP and PI blocks, but the interface between these two is not shown in the simulation. These interface shapes were calculated using the noninterpenetrating corona approximation with the PS blocks in compression. However, due to the symmetric nature of the quadratic chain conformation potential, similar results were also obtained when considering strong corona interpenetration and azimuthally dependent stretching of the PS blocks. Notice that for, large PS volume fractions, the PI–PS interface is circular in shape, but as the PS volume fraction decreases below about 0.4, the interface becomes locally flatter and the corners seen in the micrograph begin to develop. The simulation corresponding to the actual 0.33/0.33/0.33 volume fractions (curves labeled 0.3 and 0.7) is continued all the way around the illustration of the morphology in Figure 3a. Of course, as the PS volume fraction approaches zero, the PI–PS interface becomes straight and coincident with the outer edge of the simulation triangle.

The development of the flat sections and sharp corners in the PI–PS interface is the result of the constant polymer segmental density constraint forcing the PS blocks to uniformly fill the outer regions of the W–S cell. As seen in the simulation and in the micrograph, when the outer block volume is smaller than about 40%, the geometry of the outer contours of the W–S cell is effectively transferred to the PS–PI interface via the chain conformational potential. When the volume of the outer block is much larger, as in the many A/B diblock cylindrical systems previously studied, the IMDS is effectively screened from the W–S cell geometry by the longer outer block chains. This can be qualitatively appreciated by examining eq 2. If the outer blocks become relatively short such that R_{j0} is relatively small, then the energetic penalty for a deformation of absolute value $|R_j - R_{j0}|$ will be correspondingly magnified. Short chains act as stiffer entropy springs than long chains when compared for a given absolute displacement (either tension or compression), and thus these short chains are more effective in transferring the effects of the outer W–S cell geometry to the PS–PI interface.

Quite analogous interfacial curvature behavior has been demonstrated for the inverse hexagonal phase (H_{II}) in lipid–water systems. The H_{II} phase consists of a set of hexagonally arranged cylinders of water surrounded by a lipid–hydrocarbon matrix.[41] Gruner and co-workers observed increased thermodynamic stability of the H_{II} phase upon the addition of small amounts of alkanes[42] or upon the addition of longer chain lipids.[43] Such effects were explained via chain-packing requirements such that the free alkane or the longer chain lipid molecules preferentially distributed to the corners of the W–S cell to relieve the chain stretching of the major lipid component. Recent work by Gruner et al.[44] used Fourier reconstruction of the X-ray diffraction spectra to explicitly show a 5–10% radial deviation from circularity of the electron density distribution at the lipid–water interface. Addition of an alkane allowed the interface to relax to a circular geometry. Furthermore, preferential localization of the alkane at the corner regions of the W–S cell was also shown by SANS employing a deuterated alkane.[45]

The effect of the W–S cell geometry on the IMDS shape has not been observed in previous studies of cylindrical diblock compolymer morphologies because these materials form equilibrium structures where the outer block which contacts the corners of the W–S cell is always the major component with a volume fraction typically larger than 60%. In the 33/33/33 ABC triblock used in the present study the system morphology is forced to have a much shorter block in the matrix phase leading to the interesting, pointed hexagonal structures in a totally amorphous, well-ordered, block copolymer system.

We would expect to see other non-CMC IMDS's in block copolymer systems when the following criteria are satisfied: The logical choice for a CMC IMDS results, as indicated in Figure 3b, in a significant variation in the domain thickness relative to the average domain thickness; the minority fraction block ($f < 0.4$) is forced to occupy this variable thickness domain region, and the total block copolymer molecular weight is relatively low. The value of relative variation in corona thickness is 0.7 for the system investigated in this paper. On the basis of this result, we expect non-CMC interfaces when $(L_{max}-L_{min})/L_{av}$ is approximately 0.7 or greater.

Acknowledgment. We thank L. J. Fetters of Exxon for synthesizing the triblock copolymer used in this study. S.P.G. wishes to thank R. Kusner, D. Hoffman, and the other organizers of the NSF Regional Geometry Institute during the summer of 1991. It was at this meeting, through the help of K. Brakke, that the Surface Evolver was first applied to block copolymers. This work was supported by the National Science Foundation Polymers Program (Grant DMR-8907433) and the Center for Materials Science and Engineering at the Massachusetts Institute of Technology (National Science Foundation Grant 9022933).

References and Notes

(1) Kinning, D. J.; Thomas, E. L.; Ottino, J. M. *Macromolecules* **1987**, *20*, 1129.
(2) Alward, D. B.; Kinning, D. J.; Thomas, E. L.; Fetters, L. J. *Macromolecules* **1986**, *19*, 215.
(3) Sax, J.; Ottino, J. M. *Polym. Eng. Sci.* **1983**, *23*, 165.
(4) Thomas, E. L.; Gido, S. P. In *Materials Research Society Symposium Proceedings*; Buckley, A., Gallagher-Daggitt, G., Karasz, F. E., Ulrich, D. R., Eds.; Materials Research Society: Pittsburgh, PA, 1990; Vol 175, p 315.
(5) Gido, S. P. Ph. D. Thesis, Massachusetts Institute of Technology, Cambridge, MA, 1993.
(6) Helfand, E.; Wasserman, Z. R. *Macromolecules* **1976**, *9*, 879.
(7) Hashimoto, T.; Shibayama, M.; Kawai, H. *Macromolecules* **1980**, *13*, 1237.
(8) Hashimoto, T.; Fujimura, M.; Kawai, H. *Macromolecules* **1980**, *13*, 1660.
(9) Hashimoto, H.; Fujimura, M.; Hashimoto, T.; Kawai, H. *Macromolecules* **1981**, *14*, 844.
(10) Bates, F. S.; Berney, C. V.; Cohen, R. E. *Macromolecules* **1983**, *16*, 1101.
(11) Thomas, E. L.; Anderson, D. M.; Henkee, C. S.; Hoffman, D. *Nature* **1988**, *334*, 598.
(12) Gido, S. P.; Gunther, J.; Thomas, E. L.; Hoffman, D., submitted to *Macromolecules*.
(13) Hashimoto, T.; Koizumi, S.; Hasegawa, H.; Izumitani, T.; Hyde, S. T. *Macromolecules* **1992**, *25*, 1433.
(14) Helfand, E.; Tagami, Y. *J. Chem. Phys.* **1972**, *56*, 3592.
(15) Helfand, E. *J. Chem. Phys.* **1975**, *63*, 2192.
(16) Hoffman, D., personal communication.
(17) Sadoc, J. F.; Charvolin, J. *J. Phys. (Paris)* **1986**, *47*, 683.
(18) Charvolin, J.; Sadoc, J. F. *J. Phys. (Paris)* **1987**, *48*, 1559.
(19) Semenov, A. N. *Sov. Phys. JETP* **1985**, *61*, 733.
(20) Helfand, E. *Acc. Chem. Res.* **1975**, *8*, 297.
(21) Helfand, E.; Wasserman, Z. R. *Polym. Eng. Sci.* **1977**, *17*, 582.
(22) Helfand, E.; Wasserman, Z. R. *Macromolecules* **1980**, *13*, 994.
(23) Hadziioannou, G.; Mathis, A.; Skoulios, A. *Colloid Polym. Sci.* **1979**, *257*, 22.
(24) Hadziioannou, G.; Skoulios, A. *Macromolecules* **1982**, *15*, 267.
(25) Hashimoto, T.; Shibayama, M.; Kawai, H.; Watanabe, H.; Kotaka, T. *Macromolecules* **1983**, *16*, 361.
(26) Milner, S. T.; Witten, T. A.; Cates, M. E. *Macromolecules* **1988**, *21*, 2610.
(27) Zhulina, E. B.; Liatskaya, Y. V.; Birshtein, T. M. *Polymer* **1992**, *33*, 332.
(28) Anderson, D. M.; Thomas, E. L. *Macromolecules* **1988**, *21*, 3221.
(29) Thomas, E. L.; Alward, D. B.; Kinning, D. J.; Martin, D. C.; Handlin, D. L., Jr.; Fetters, L. J. *Macromolecules* **1986**, *19*, 2197.
(30) Gonçalves, M. C.; Gobran, D. A.; Schwark, D. W.; Thomas, E. L.; Fetters, L. J., in preparation for *Polymer*.
(31) Riess, G.; Schlienger, M.; Marti, G. *J. Macromol. Sci., Phys.* **1980**, *B17*, 355.
(32) Leibler, L.; Orland, H.; Wheeler, J. C. *J. Chem. Phys.* **1983**, *79*, 3550.
(33) Mogi, Y.; Kotsuji, H.; Kaneko, Y.; Mori, K.; Matsushita, Y. *Macromolecules* **1992**, *25*, 5408.
(34) Mogi, Y.; Mori, K.; Matsushita, Y.; Noda, I. *Macromolecules* **1992**, *12*, 5412.
(35) Milner, S. T. *Science* **1991**, *251*, 905.
(36) Mori, K.; Hasagawa, H.; Hashimoto, T. *Polym. J.* **1985**, *17*, 799.
(37) de Gennes, P.-G. *J. Phys. (Paris)* **1976**, *37*, 1443.
(38) de Gennes, P.-G. *Macromolecules* **1980**, *13*, 1069.
(39) Alexander, S. *J. Phys.* **1977**, *38*, 977.
(40) Brakke, K. A. *Surface Evolver Manual*, Geometry Supercomputer Project of the University of Minnesota, 1991.
(41) Luzzati, V.; Husson, F. *J. Cell Biol.* **1962**, *12*, 207.
(42) Kirk, G. L.; Gruner, S. M. *J. Phys.* **1985**, *46*, 761.
(43) Tate, M. W.; Gruner, S. M. *Biochemistry* **1987**, *26*, 231.
(44) Turner, D. C.; Gruner, S. M. *Biochemistry* **1992**, *31*, 1340.
(45) Turner, D. C.; Gruner, S. M.; Huang, J. *Biochemistry* **1992**, *31*, 1356.